**Supplementary information**

# Boosting the photoluminescent properties of protein-stabilized gold nanoclusters through protein engineering

Antonio Aires, Ahmad Sousaraei, Marco Möller, Juan Cabanillas-Gonzalez, and Aitziber L. Cortajarena*

## Materials and Methods

### Protein Design, Cloning and Molecular Biology

Consensus tetratricopeptide repeat (CTPR) proteins were generated and characterized as previously described.[1, 2] The engineered CTPR proteins were generated by the assembly of different number of the designed repeat modules, wildtype module ($W_1$), W_E2H_N6H module ($C_{2His}$), W_E2H_N6H_N9H_Y12L_K13H module ($C_{4His}$), W_E2C_N6C module ($C_{2Cys}$), W_E2C_N6C_N9C_Y12L_K13C module ($C_{4Cys}$), W_E2W_N9H module ($W_{2Trp}$) and W_E2C_N6C_N9C_Y12L_K13C_Y17W_D31W module ($C_{4Cys\_2Trp}$) having an extra sequence at the N-terminal end due to the cloning strategy (GAMGS), and an additional helix at the C-terminal end for improved solubility (AEAKQNLGNAKQKQG). $C_{2His}$ module ($H_1$) (AHAWYHLGNAYYKQGDYDEA IEYYQKALELDPRS), $C_{4His}$ ($H_2$) module (AHAWYHLGHAYLHQGDYDEAIEYYQK ALELDPRS), $C_{2Cys}$ ($C_1$) module (ACAWYCLGNAYYKQGDYDEAIEYYQ KALELDPRS), $C_{4Cys}$ module ($C_2$) (ACA WYCLGCAYLHQGDYDEAIEYYQKALEL DPRS), $W_{2Trp}$ ($W_2$) module (AWAWYNLGWAYYKQGDYDEAIEYYQKALELDPR S) and $C_{4Cys\_2Trp}$ ($C_3$) module (ACAWYCLGCAYLCQGDWDEAIEYYQKALELWP RS) were generated from the previously described $W_1$ module (AEAWYNLGNA YYKQGDYDEAIEYYQKALELDPRS) by QuikChange Site-Directed mutagenesis. A series of engineered CTPR proteins were created by the combination of the modules $W_1$,

$H_1$, $H_2$, $C_1$, $C_2$, $C_3$, and $W_2$: CTPR3-$W_1H_1W_1$ (C3-2His), CTPR3-$W_1C_1W_1$ (C3-2Cys), CTPR3-$W_1H_2W_1$ (C3-4His), CTPR3-$W_1C_2W_1$ (C3-4Cys), CTPR4-$W_1(H_1)_2W_1$ (C4-2His), CTPR4-$W_1(C_1)_2W_1$ (C4-4Cys), CTPR4-$W_1(H_2)_2W_1$ (C4-8His), CTPR4-$W_1(C_2)_2W_1$ (C4-8Cys), CTPR5-$W_1(H_1)_3W_1$ (C5-6His), CTPR5-$W_1(C_1)_3W_1$ (C5-6Cys), CTPR5-$W_1(H_2)_3W_1$ (C5-12His), CTPR5-$W_1(C_2)_3W_1$ (C5-12Cys), CTPR6-$W_1(H_1)_4W_1$ (C6-8His), CTPR6-$W_1(C_1)_4W_1$ (C6-8Cys), CTPR6-$W_1(H_2)_4W_1$ (C6-16His), CTPR6-$W_1(C_2)_4W_1$ (C6-16Cys), CTPR7-$W_1(C_2)_5W_1$ (C7-20Cys), CTPR8-$W_1(C_2)_6W_1$ (C8-24Cys), CTPR6-$W_2(C_2)_4W_2$ (C6-16Cys-4W), CTPR6-$W_2(C_3)_4W_2$ (C6-16Cys-12W), CTPR7-$W_2(C_3)_5W_2$ (C7-20Cys-14W) and CTPR8-$W_2(C_2)_6W_2$ (C8-24Cys-16W) (Table S1). For this purpose, DNA encoding the W, H, $H_2$, C, $C_2$, $C_3$, and $W_2$ modules were fused using a modular cloning strategy based on BamHI and BglII digestion.[3] The genes encoding the generated CTPR proteins were cloned into the pProEx-HTA vector and their identities verified by DNA sequencing (Stab Vida).

**Table S1.** Metal-binding proteins generated by assembly of GCM and wild type modules.

| Scaffold | Acronym | N ($W_{1-2}$) | GCM | N (GCM) |
|---|---|---|---|---|
| CTPR3-$(W_1)_3$ | C3 | 3 $W_1$ | -- | 0 |
| CTPR3-$W_1H_1W_1$ | C3-2His | 2 $W_1$ | $H_1$ | 1 |
| CTPR3-$W_1C_1W_1$ | C3-2Cys | 2 $W_1$ | $C_1$ | 1 |
| CTPR3-$W_1H_2W_1$ | C3-4His | 2 $W_1$ | $H_2$ | 1 |
| CTPR3-$W_1C_2W_1$ | C3-4Cys | 2 $W_1$ | $C_2$ | 1 |
| CTPR4-$(W_1)_4$ | C4 | 4 $W_1$ | -- | 0 |
| CTPR4-$W_1(H_1)_2W_1$ | C4-4His | 2 $W_1$ | $H_1$ | 2 |
| CTPR4-$W_1(C_1)_2W_1$ | C4-4Cys | 2 $W_1$ | $C_1$ | 2 |
| CTPR4-$W_1(H_2)_2W_1$ | C4-8His | 2 $W_1$ | $H_2$ | 2 |
| CTPR4-$W_1(C_2)_2W_1$ | C4-8Cys | 2 $W_1$ | $C_2$ | 2 |

| | | | | |
|---|---|---|---|---|
| CTPR5-$(W_1)_5$ | C5 | 5 $W_1$ | -- | 0 |
| CTPR5-$W_1(H_1)_3W_1$ | C5-6His | 2 $W_1$ | $H_1$ | 3 |
| CTPR5-$W_1(C_1)_3W_1$ | C5-6Cys | 2 $W_1$ | $C_1$ | 3 |
| CTPR5-$W_1(H_2)_3W_1$ | C5-12His | 2 $W_1$ | $H_2$ | 3 |
| CTPR5-$W_1(C_2)_3W_1$ | C5-12Cys | 2 $W_1$ | $C_2$ | 3 |
| CTPR6-$(W_1)_6$ | C6 | 6 $W_1$ | -- | 0 |
| CTPR6-$W_1(H_1)_4W_1$ | C6-8His | 2 $W_1$ | $H_1$ | 4 |
| CTPR6-$W_1(C_1)_4W_1$ | C6-8Cys | 2 $W_1$ | $C_1$ | 4 |
| CTPR6-$W_1(H_2)_4W_1$ | C6-16His | 2 $W_1$ | $H_2$ | 4 |
| CTPR6-$W_1(C_2)_4W_1$ | C6-16Cys | 2 $W_1$ | $C_2$ | 4 |
| CTPR6-$W_2(C_3)_4W_2$ | C6-16Cys-12Trp | 2 $W_2$ | $C_3$ | 4 |
| CTPR7-$W_1(C_2)_5W_1$ | C7-20Cys | 2 $W_1$ | $C_2$ | 5 |
| CTPR7-$W_2(C_3)_5W_2$ | C7-20Cys-14Trp | 2 $W_2$ | $C_3$ | 5 |
| CTPR8-$W_1(C_2)_6W_1$ | C8-24Cys | 2 $W_1$ | $C_2$ | 6 |
| CTPR8-$W_2(C_3)_2W_1$ | C8-24Cys-16Trp | 2 $W_2$ | $C_3$ | 6 |

N: number of $W_1$ or $W_2$ capping modules; GCM: gold coordination modules.

**Protein Expression and Purification**

Synthetic genes for the desired proteins in pProEx-HTA vectors, coding for N-terminal hexahistidine tag and ampicillin resistance, were expressed in *Escherichia coli* C41 (DE3) after induction with 1 mM isopropyl β-d-thiogalactoside (IPTG) at an optical density of 0.6-0.8 followed by 18 h growth at 20°C. The cell pellets were resuspended in lysis buffer (500 mM sodium chloride, 500mM urea, 50 mM Tris pH 8.0) or lysis buffer 6 M urea (in the case of Trp containing proteins), and lysed by sonication. The proteins were purified from the supernatant using standard Ni-NTA affinity purification protocol. The N-

terminal hexahistidine tag was then cleaved from the CTPR proteins using the Tobacco Etch Virus (TEV) protease. As a final step, the aqueous solutions of CTPRs were dialyzed against phosphate saline buffer (50 mM sodium chloride, 50 mM sodium phosphate pH 7.4) at 4°C using a dialysis membrane with molecular weight cutoff of 6-8 kDa. Protein concentration was measured by UV absorbance at 280 nm.

**Synthesis of Protein-stabilized Gold Nanoclusters**

**Reduction agent-assisted procedure (reduction).** The protein-stabilized AuNCs were synthesized using a modified protocol based on a previously reported procedure.[4-7] Briefly, 1 mL of protein at 20 μM in 150 mM sodium chloride, 50 mM sodium phosphate pH 10, were mixed with $HAuCl_4$ (75 μL 10 mM, 40 eq. respect to protein) for 1hour, under shaking at room temperature. Then, the reduction of the Au ions to AuNCs was achieved by the addition of 75 μL of sodium ascorbate at 1M (100 eq. respect to Au ions). The reaction was incubated at 50°C for 72 h. Finally, the unreacted salts were removed via gel filtration using a Sephadex G-25M column and the protein-stabilized AuNCs were purified by fast protein liquid chromatography (FPLC). The purified samples were stored at 4°C. The fluorescence spectra of protein-stabilized AuNCs were collected using a Varioskan microplate reader (Thermo Scientific).

**Biomineralization-inspired procedure (biomineralization)**. The protein-stabilized AuNCs were synthesized using a modified protocol based on a previously reported procedure.[8] Briefly, 1 mL of protein at 20 μM in 150 mM sodium chloride, 50 mM sodium phosphate pH 12, were mixed with $HAuCl_4$ (2 eq. respect to the number of Au coordination residues (Cys/His)) for 24 hour, under shaking at 50ºC. Finally, the unreacted salts were removed via gel filtration using a Sephadex G-25M column and the protein-stabilized AuNCs were purified by fast protein liquid chromatography (FPLC).

The purified samples were stored at 4°C. The fluorescence spectra of protein-stabilized AuNCs were collected using a Varioskan microplate reader (Thermo Scientific).

**Steady-state optical spectroscopy**

UV-visible absorption spectra were measured in a Jasco V-630 Bio spectrophotometer. Fluorescence spectra were recorded in a LS-55 PerkinElmer spectrofluorometer with a slit of 1 nm band-pass. All the absorption and emission measurements were performed using a standard quartz cuvette of 1 cm path length. The fluorescence quantum yield ($\Phi_x$) was calculated using, anthracene in ethanol as a reference ($\Phi_{ref}$ = 0.27, $\lambda_{exc}$ = 370 nm and $\lambda_{em}$ = 423 nm) for AuNCs by reduction agent-assisted procedure, or rhodamine 6G in ethanol ($\Phi_{ref}$ = 0.94, $\lambda_{exc}$ = 488 nm and $\lambda_{em}$ = 552 nm), and the equation (1):

$$\phi_x = \phi_{ref} \ \frac{Grad_x}{Grad_{ref}} \left(\frac{\eta_x^2}{\eta_{ref}^2}\right) \textbf{(1)}$$

where $Grad_x$ and $Grad_{ref}$ are the integrated photoluminescence intensities of sample and reference normalized by their respective absorbance at excitation wavelength, for the sample and the reference, respectively, and $\eta_x$ and $\eta_{ref}$ are the refractive indexes of the solvents, PBS (150 mM NaCl, 50 mM phosphate pH 7.4) and ethanol, respectively. The ratios between the different PL emission components in the PL spectra were calculated by integrating the peak areas after the deconvolution of the spectra.

**Time–resolved photoluminescence spectroscopy**

Photoluminescence lifetime measurements were carried out with the technique of time-correlated single photon counting using three different excitation schemes. Nanosecond fluorescence lifetimes were obtained upon photoexciting with PDL 828 Picoquant Sepia diode laser delivering 50 ps pulses at 405 nm at 10 MHz repetition rate. Picosecond lifetimes, relevant for energy transfer studies, required photoexcitation with 120 fs pulses

at 258 nm obtained from the third harmonic generation of the 775 nm fundamental of a Clark-MXR femtosecond regenerative amplifier delivered at 1 KHz repetition rate. Microsecond lifetime measurements involved photoexcitation with 0.3 ns pulses at 355 nm delivered by a tripled-frequency passive Q-switch Nd:YAG laser from TEEM Photonics at a variable (0.1-1KHz) repetition rate. In all cases the photoluminescence was dispersed by a spectrometer (SP2500, Acton Research), and detected with a Picoquant PMA Hybrid-Photomultiplier Assembly with a transit time spread of less than 50 ps. Picosecond/nanosecond decays were recorded with a Picoquant Hydraharp time-correlated single photon counting (TCSPC) electronics, whereas microsecond decays were acquired with a Picoquant TimeHarp 260 Time-Correlated Single Photon Counting (TCSPC) and Multi-Channel Scaling (MCS) board. The fastest instrumental response achieved (with femtosecond pulses) was 39 ps measured from scattering of the photoexciting pulses. Measurements were carried out in solutions placed in a 2 mm-optical path quartz cuvette. PL decay curves were fitted to multi-exponential laws using a Picoquant Fluofit analysis software which provided individual decay components with their corresponding statistical weight as well as amplitude-averaged PL decay values.

**Circular Dichroism**

The protein secondary structure, of the proteins before and after the AuNCs synthesis, was examined by CD using a Jasco J-815 spectrometer (JASCO Corporation, Tokyo, Japan). CD spectra were acquired at 10 μM protein concentration in a 1 mm path length cell at 20ºC using a 1 nm bandwidth with 1 nm increments and 10 s average time.

**Matrix assisted laser desorption ionization (MALDI) mass spectrometry**

Mass spectra were acquired on an Applied Biosystems Voyager Elite MALDI-TOF mass spectrometer with delayed extraction (Applied Biosystems, Framingham, MA, USA)

equipped with a pulsed $N_2$ laser (λ= 337 nm). Sinapic acid was used as matrix. An extraction voltage of 20 kV was used. All mass spectra were acquired in positive reflection mode using delayed extraction with an average of 50−100 laser shots. MALDI-TOF sample preparation included 1 μL of the sample mixed with 4 μL of sinapic acid in 50:50 water/acetonitrile with 0.01% TFA. Then, 2 μL of the mixture was deposited onto the MALDI plate and allowed to air-dry. The instrument was externally calibrated using monoisotopic peaks from the sinapic acid matrix (MH+ at m/z 225.071).

**X-ray photoelectron spectroscopy (XPS)**

X-ray photoelectron spectroscopy measurements were performed with a SPECS SAGE HR 100 spectrometer equipped with a 100 mm mean radius PHOIBOS analyzer and a non-monochromatic X-ray source (Mg Kα line of 1253.6 eV energy and 250 W), placed perpendicular to the analyzer axis and calibrated using the 3d5/2 line of Ag, with a full width at half maximum of 1.1 eV. All measurements were made in an ultrahigh vacuum chamber at a pressure of around $8 \times 10^{-8}$ mbar. An electron flood gun was used to neutralize for charging. Measurements were conducted directly on dry deposited films, which were previously washed with absolute ethanol and cut into samples of 1 cm × 1 cm. The analysis of spectra was done with CasaXPS 2.3.15dev87 software.

**Transmission Electron Microscopy (TEM)**

Ultrathin carbon films on holey carbon support film, 400 mesh copper grids (TED PELLA INC.) were exposed to glow discharge treatment before sample deposition. TEM samples were prepared by depositing 0.4 μL of the sample solution on the grid. Micrographs were recorded using a JEOL JEM 2100F electron microscope operating at 200 kV with a Field Emission Gun equipped with an INCA x-sight energy dispersive X-ray radiation (EDX) detector (Oxford Instruments) to analyze the elemental composition of the material.

HAADF STEM images were acquired on a JEOL JEM-2100F UHR microscope at 200 kV in scanning mode, with a probe size of 0.2 nm and a choice of the camera length that ensures an inner detector angle of 75 mrad (HAADF) to enhance the contrasts of the metal atoms on the carbon support film. The particle size distribution was determined from TEM micrographs using ImageJ software measuring the diameter of a total of 200 AuNCs.

## Results and Discussion

### Characterization of the Prot-AuNCs synthesized through a reduction agent-assisted procedure (reduction)

### MALDI-TOF MS

**Table S2.** Determination of the number of Au atoms in the Prot-AuNCs synthesized through reduction by MALDI-TOF.

| Sample | MALDI-TOF | | |
|---|---|---|---|
| | MSC[a] | FWHM[b] | NMA[c] |
| C3-4Cys | 13952.98 | 15 | -- |
| C3-4Cys-AuNCs | 14219.75 | 643 | 5±3 |
| C4-8Cys | 17851.68 | 32 | -- |
| C4-8Cys-AuNCs | 19397.83 | 853 | 8±4 |
| C5-12Cys | 21760.77 | 51 | -- |
| C5-12Cys-AuNCs | 24120.59 | 908 | 11±5 |
| C6-16Cys | 25669.10 | 64 | -- |
| C6-16Cys-AuNCs | 28411.94 | 1318 | 14±7 |
| C7-20Cys | 29581.11 | 18 | -- |
| C7-20Cys-AuNCs | 32823.02 | 1558 | 15±8 |
| C8-24Cys | 33459.51 | 156 | -- |
| C8-24Cys-AuNCs | 37565.89 | 1361 | 21±7 |

*[a]Center of mass peak in Daltons (MSC). [b]Full width at half maximum in Daltons (FWHM). [c] Number of metal atoms per cluster (NMA).*

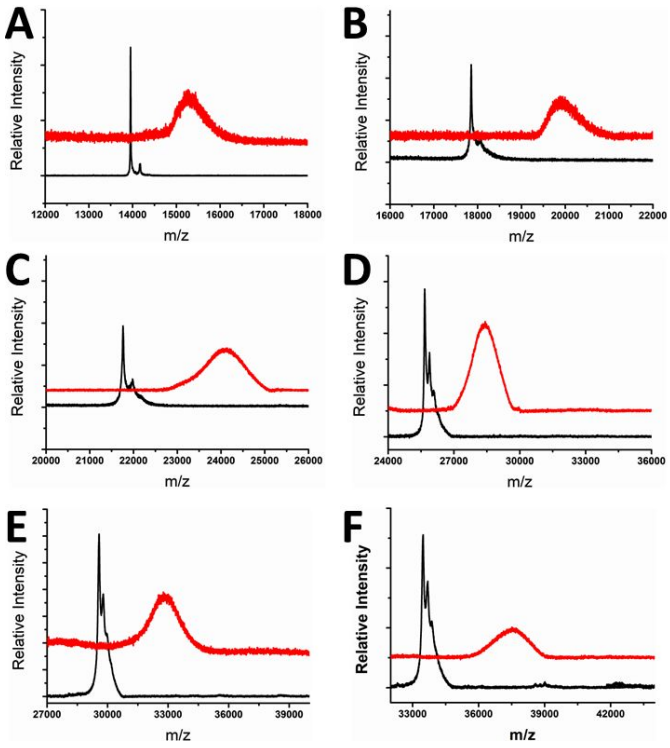


**Figure S1.** MALDI-TOF mass spectra of metal binding proteins (black lines) and protein-stabilized AuNCs (red lines) synthesized through reduction. **A**. C3-4Cys protein and C3-4Cys-AuNCs. **B**. C4-8Cys protein and C4-8Cys-AuNCs. **C**. C5-12Cys proteins and C5-12Cys-AuNCs. **D**. C6-16Cys protein and C6-16Cys-AuNCs. **E**. C7-20Cys protein and C7-20Cys-AuNCs. **F**. C8-24Cys protein and C8-24Cys-AuNCs.

## Scanning Transmission Electron Microscopy (HAADF-STEM)

The size and morphology of the C8-24Cys-AuNCs was evaluated by scanning transmission electron microscopy (STEM), taking advantage of the chemical contrast of Au obtained in high-angle annular dark field (HAADF) (Figure S2A). Indeed, C8-24Cys-AuNCs showed NCs with an average diameter of 1.2 ± 0.3 nm (Figure S2B). This size regime is accordant with the size range of previously reported fluorescent AuNCs.[9, 10]

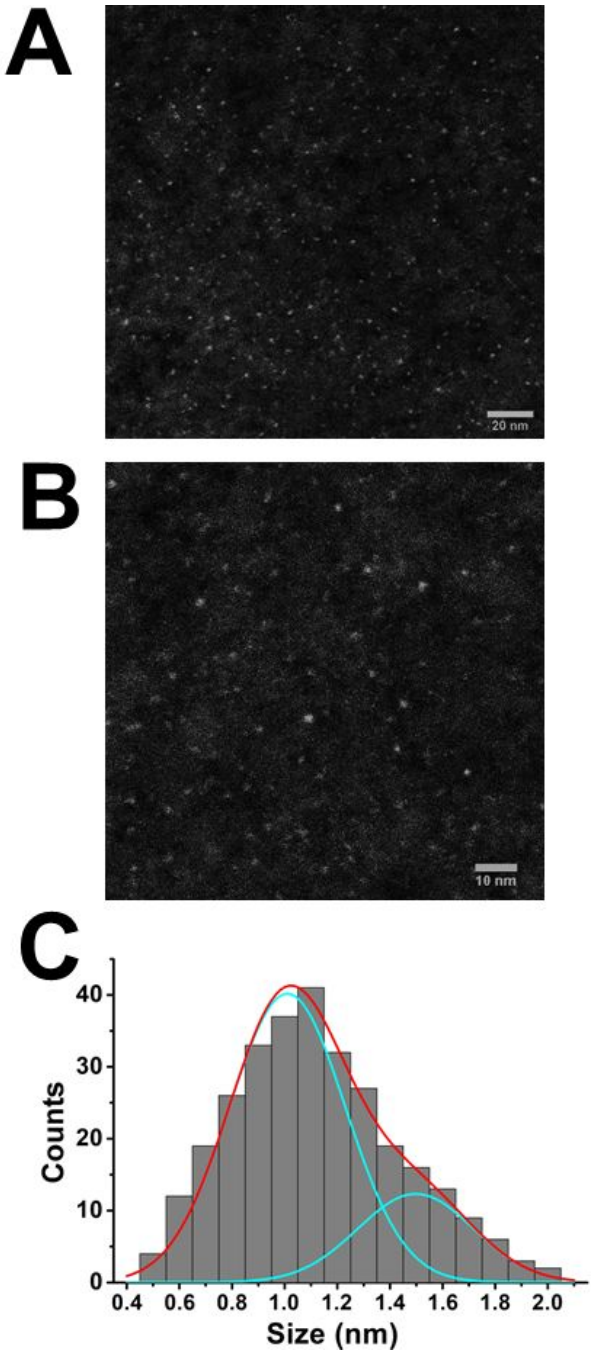


**Figure S2**. (A-B) HAADF STEM images of C8-24Cys-AuNCs synthesized by reduction. Scale bar: 20 and 10nm. (C) Size distribution histogram of C6-16Cys-AuNCs measured from STEM micrographs. The histogram was fitted to a two-component Gaussian distribution (R-squared = 0.99). The ratios between the two size populations were calculated from the size-distribution histogram by integrating the peak areas.

## Circular Dichroism (CD)

The structural integrity of the C8-24Cys protein upon AuNCs synthesis through reduction, critical for future applications, was monitored by circular dichroism (CD). CD

spectra of the C8-24Cys-AuNCs showed that the protein retained α-helical structure, indicating that the synthesis of AuNCs did not affect the structure of the scaffolds (Figure S3).

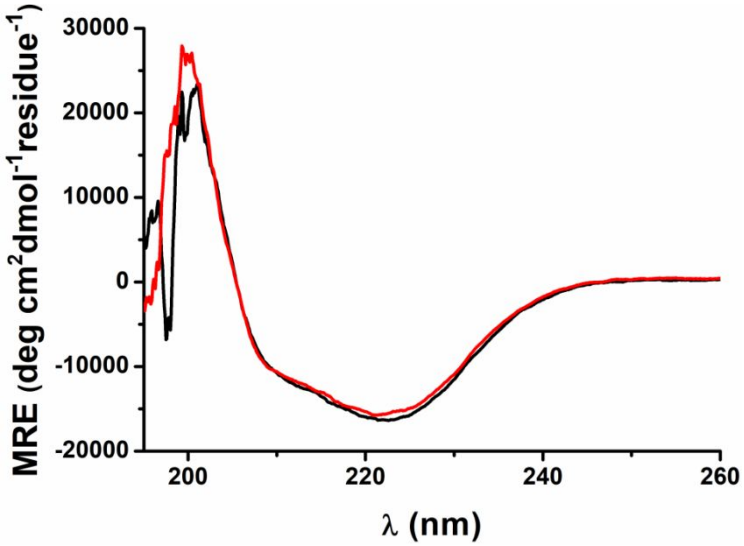


**Figure S3.** CD spectra of C8-24Cys protein (black line) and C8-24Cys-AuNCs (red line).

## Time-resolved Photoluminescence Measurements

**Table S3**. PL decay parameters for the different Prot-AuNCs synthesized by reduction.

| AuNCs | A1 | τ1 | A2 | τ2 | A3 | τ3 | A4 | τ 4 | < τ > |
|---|---|---|---|---|---|---|---|---|---|
| C8-24Cys-AuNCs ($\lambda_{em}$ 470 nm) | 72% | 0.31 ns | 26% | 2.51 ns | 2% | 10.28 ns | - | - | 1.11 ns |
| C8-24Cys-AuNCs ($\lambda_{em}$ 690 nm) | 40% | 0.12 μs | 32% | 0.66 μs | 21% | 2.67 μs | 7% | 7.41 μs | 1.37 μs |

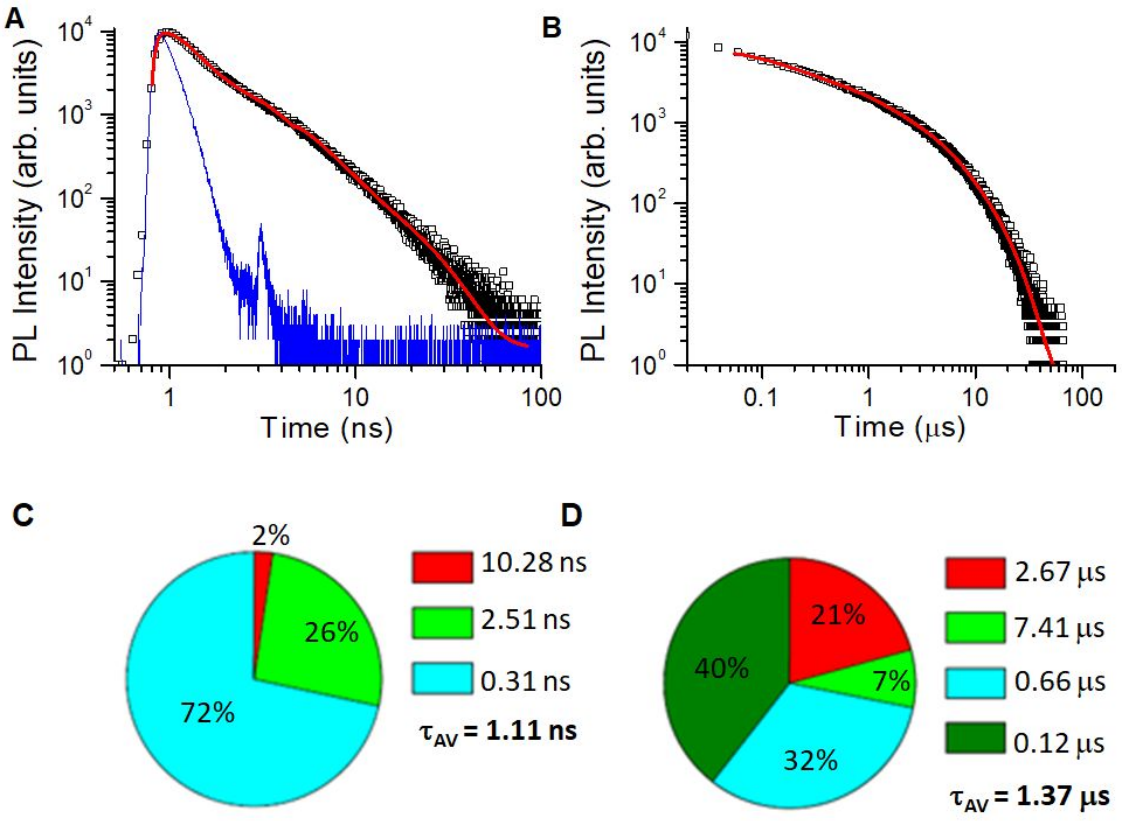


**Figure S4.** The photoluminescence lifetime analysis of C8-24Cys-AuNCs synthesized by reduction. PL decay curves with corresponding multi-exponential fits depicted by a solid red line photoexcited at 405 nm and detected at 470 nm (A) and photoexcited at 355 nm and detected at 690 nm (B). Corresponding statistical distribution of decay times are shown in C and D respectively. Nanosecond PL decays were deconvoluted by the instrumental response function (blue decay curve in A).

## X-ray photoelectron spectroscopy (XPS)

The valence state of the Prot-AuNCs was investigated by XPS. Figure S5 shows that the Au core was composed of Au (I) and Au (0). The XPS spectrum of C8-24cys-AuNCs showed a peak at the binding energy of 84.3 eV (Au $4f_{7/2}$). To further determine the Au oxidation states, the quantitative deconvolution of the Au $4f_{7/2}$ peak was performed. It could be well-deconvoluted into Au(I) and Au(0) components with binding energies of 84.5 and 83.5 eV, respectively (Figure S5). On the basis of the area ratio between these two peaks, the Au(I):Au(0) ratio was determined to be 65:35.

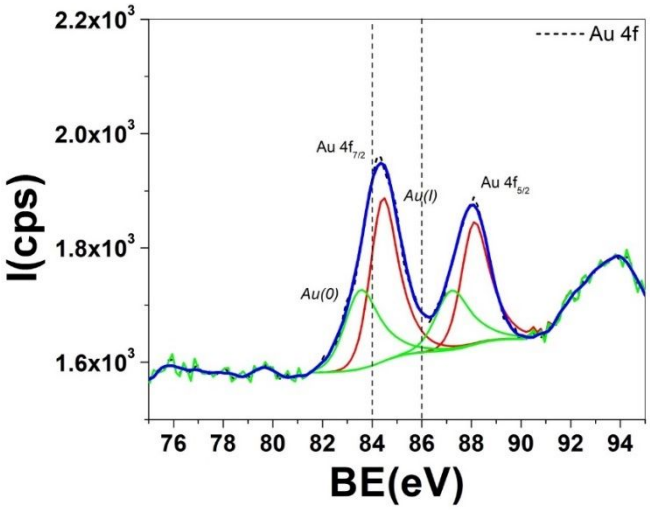


**Figure S5.** XPS spectrum of C8-24Cys$_s$-AuNCs synthesized by reduction.

## Characterization of the Prot-AuNCs synthesized through a biomineralization-inspired procedure (Biomineralization)

### MALDI-TOF MS

**Table S4.** Determination of the number of Au atoms in the Prot-AuNCs synthesized through a biomineralization-inspired procedure by MALDI-TOF.

| Sample | MALDI-TOF | | |
|---|---|---|---|
| | MSC[a] | FWHM[b] | NMA[c] |
| C3-4Cys | 13952.98 | 15 | -- |
| C3-4Cys-AuNCs | 16420.82 | 677 | 13±3 |
| C4-8Cys | 17851.68 | 32 | -- |
| C4-8Cys-AuNCs | 21053.19 | 801 | 16±4 |
| C5-12Cys | 21760.77 | 51 | -- |
| C5-12Cys-AuNCs | 25260.63 | 984 | 18±5 |
| C6-16Cys | 25669.10 | 64 | -- |
| C6-16Cys-AuNCs | 29613.28 | 1056 | 20±5 |
| C7-20Cys | 29581.11 | 18 | -- |
| C7-20Cys-AuNCs | 33957.72 | 1201 | 22±6 |
| C8-24Cys | 33459.51 | 156 | -- |
| C8-24Cys-AuNCs | 38271.98 | 1398 | 24±7 |

*[a]Center of mass peak in Daltons (MSC). [b]Full width at half maximum in Daltons (FWHM). [c] Number of metal atoms per cluster (NMA).*

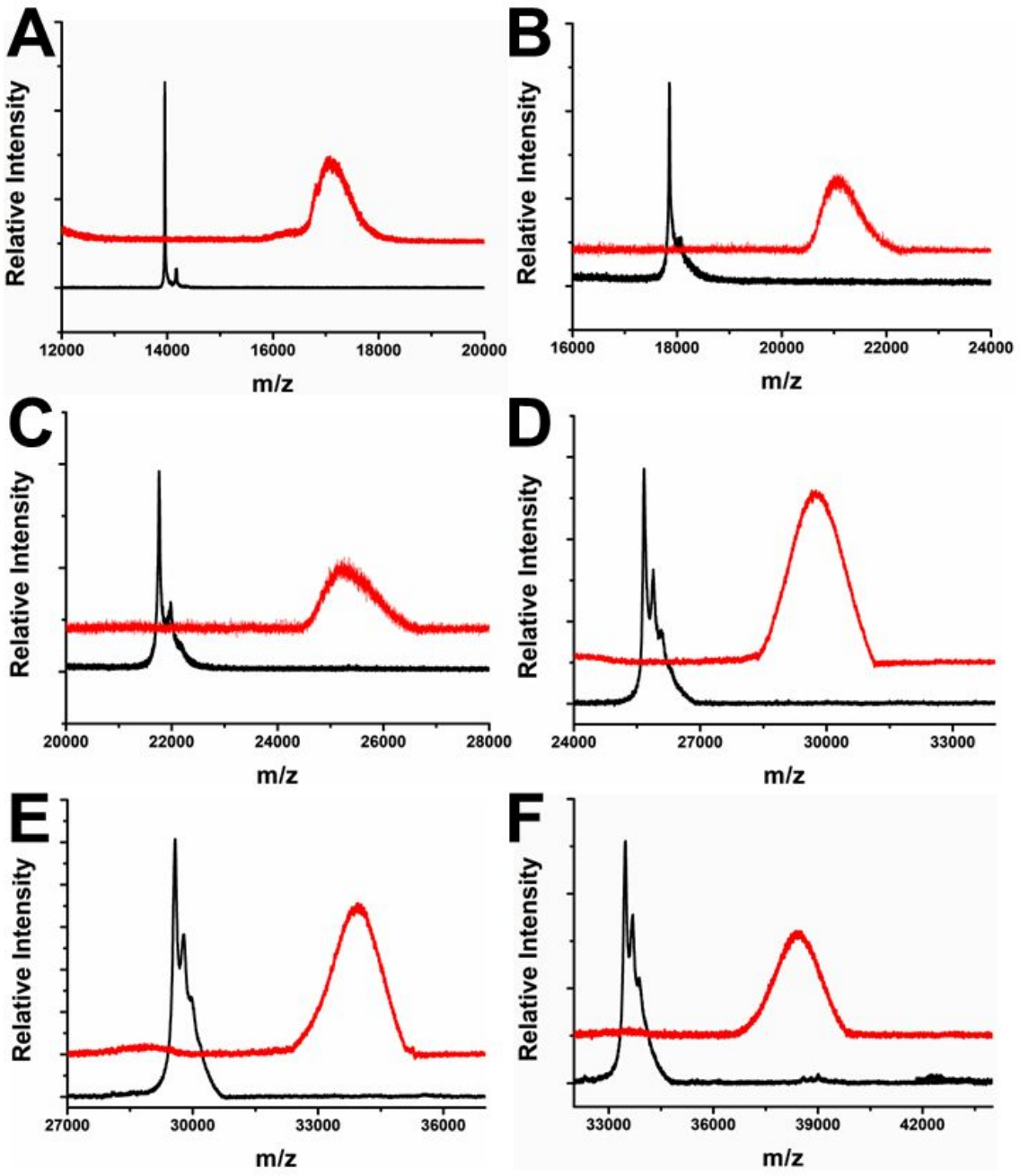


**Figure S6.** MALDI-TOF mass spectra of metal binding proteins (black lines) and protein-stabilized AuNCs (red lines) synthesized through biomineralization. **A**. C3-4Cys protein and C3-4Cys-AuNCs. **B**. C4-8Cys protein and C4-8Cys-AuNCs. **C**. C5-12Cys proteins and C5-12Cys-AuNCs. **D**. C6-16Cys protein and C6-16Cys-AuNCs. **E**. C7-20Cys protein and C7-20Cys-AuNCs. **F**. C8-24Cys protein and C8-24Cys-AuNCs.

**Scanning Transmission Electron Microscopy (HAADF-STEM)**

The size and morphology of the C8-24Cys-AuNCs was evaluated by scanning transmission electron microscopy (STEM), taking advantage of the chemical contrast of

Au obtained in high-angle annular dark field (HAADF) (Figure S7A). Indeed, C8-24CysAuNCs showed NCs with an average diameter of 1.5 ± 0.3 nm (Figure S7B). This size regime is accordant with the size range of previously reported fluorescent AuNCs.[9, 10]

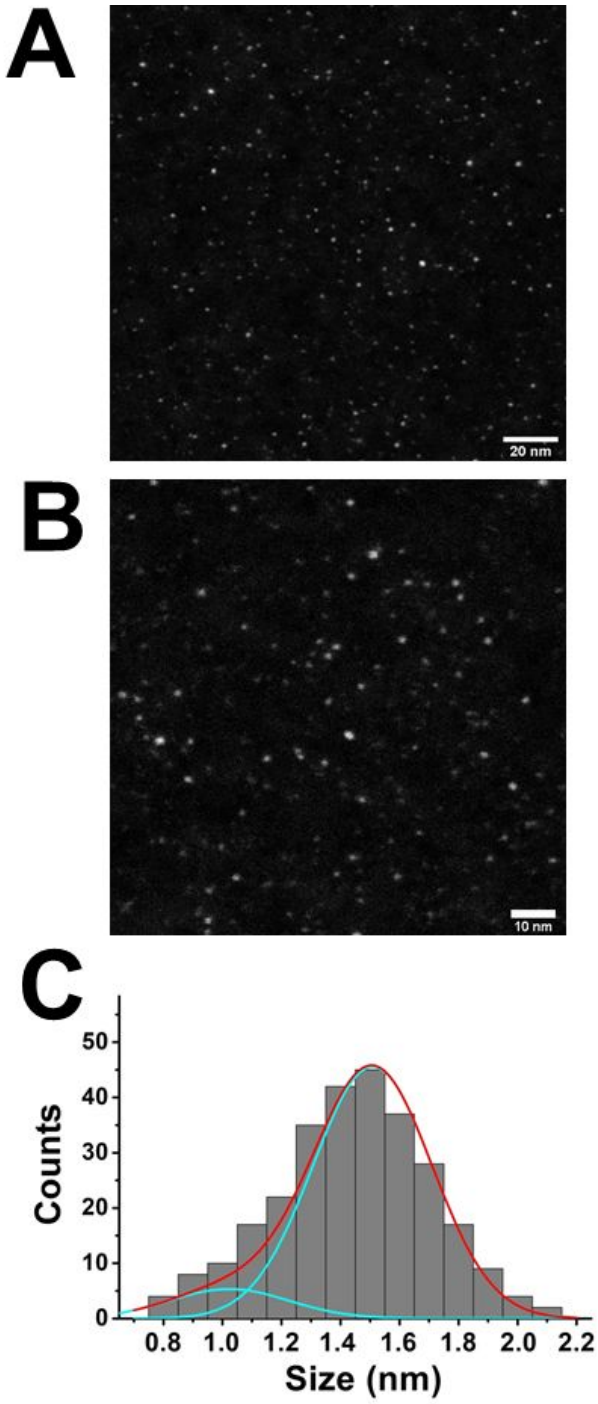


**Figure S7**. (A-B) HAADF STEM images of C8-24Cys-AuNCs synthesized by biomineralization. Scale bar: 20 and 10 nm. (C) Size distribution histogram of C8-24Cys-AuNCs measured from STEM micrographs. The histogram was fitted to a two-component Gaussian distribution (R-squared = 0.99).

## Circular Dichroism (CD)

The structural integrity of the C8-24Cys protein upon AuNCs synthesis through biomineralization, critical for future applications, was monitored by circular dichroism (CD). CD spectra of the C8-24Cys-AuNCs showed that the protein retained α-helical structure, indicating that the synthesis of AuNCs did not affect the structure of the scaffolds (Figure S8).

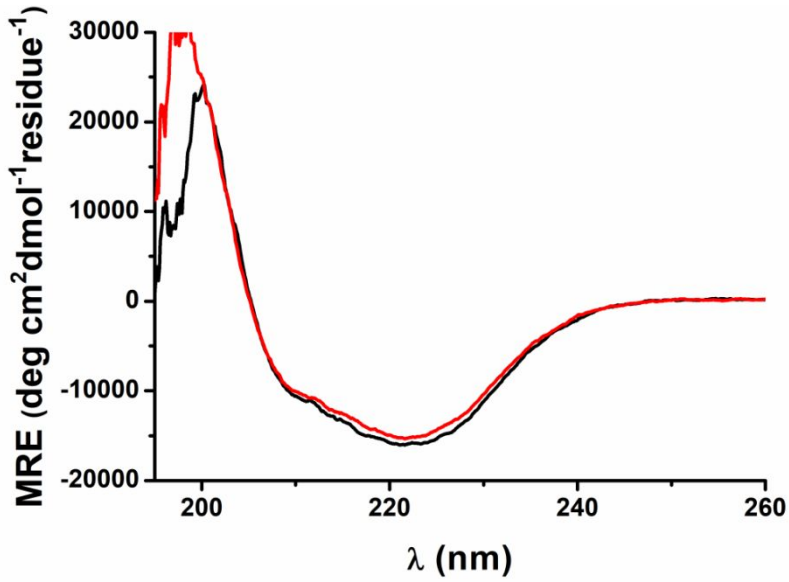


**Figure S8.** CD spectra of C8-24Cys protein (black line) and C8-24Cys-AuNCs synthesized by biomineralization (red line).

## Time-resolved Photoluminescence Measurements

**Table S5**. PL decay parameters for the different Prot-AuNCs synthesized by biomineralization.

| AuNCs | A1 | τ1 | A2 | τ2 | A3 | τ3 | < τ > |
|---|---|---|---|---|---|---|---|
| C8-24Cys-AuNCs ($\lambda_{em}$ 460 nm) | 87% | 0.16 ns | 12% | 0.52 ns | 1% | 5.10 ns | 0.22 ns |
| C8-24Cys-AuNCs ($\lambda_{em}$ 676 nm) | 26% | 0.30 μs | 55% | 1.54 μs | 19% | 3.23 μs | 1.54 μs |

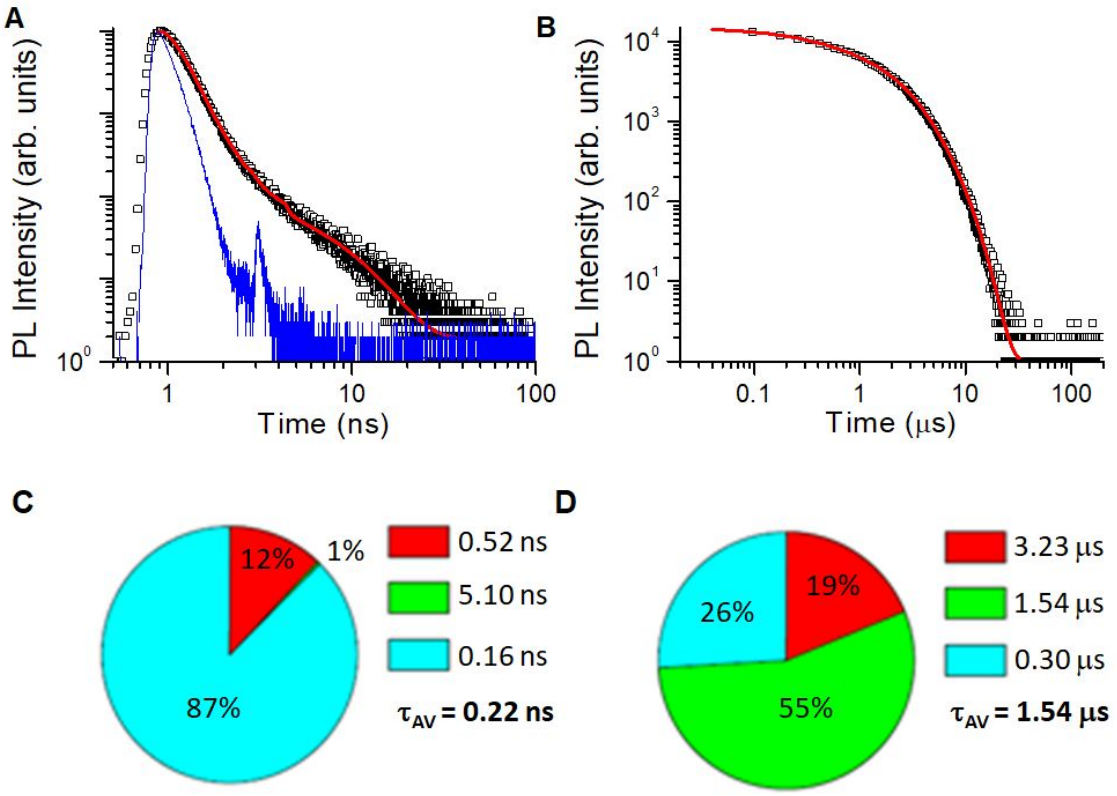


**Figure S9.** The PL lifetime analysis of C8-24Cys-AuNCs synthesized with the biomineralization-inspired procedure. PL decay curves with corresponding three-exponential fits depicted by a red solid line photoexcited at 405 nm and detected at 460 nm (A) and photoexcited at 355 nm and detected at 676 nm (B). Corresponding statistical distributions of the decay components are depicted in C and D respectively. Nanosecond PL decays were deconvoluted by the instrumental response function (blue decay curve in A).

**Phosphorescence emission of C8-24cys-AuNCs synthesized by biomineralization**

The emission spectra of the C8-24cys-AuNCs were monitored before and after of purging the C8-24cys-AuNCs solution with nitrogen and after injecting oxygen in the C8-24cys-AuNCs solution. As shown the Figure S10, the emission of the C8-24cys-AuNCs was oxygen dependent. Therefore, this measurement confirmed that the red emission band centered around 680 nm in C8-24cys-AuNCs is due to phosphorescence, in contrast with oxygen-independent PL band with maximum around 400 nm ascribed to fluorescence.

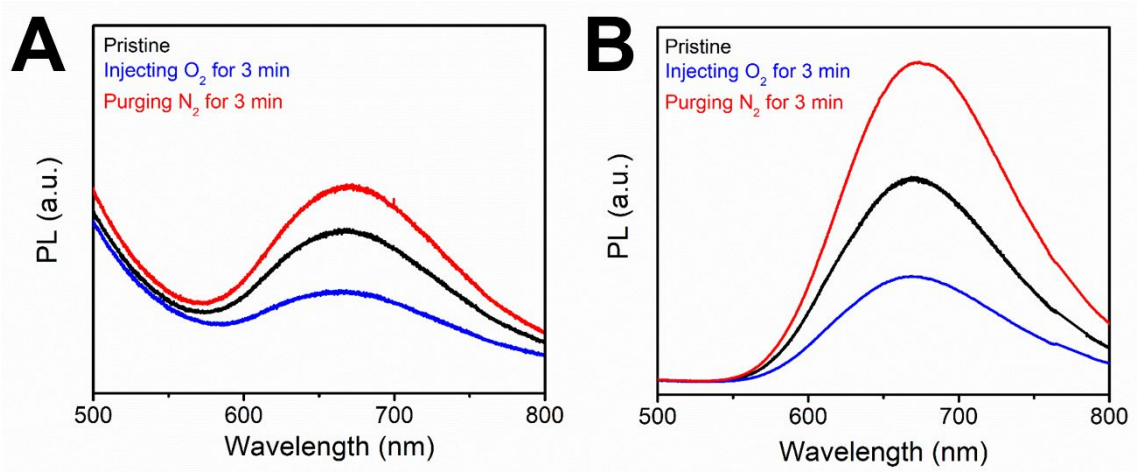


**Figure S10.** PL spectra of the C8-24Cys-AuNCs synthesized by reduction (A) and biomineralization (B) in solution and environment conditions (black line), after purging the solution with nitrogen (red line) and after injecting oxygen in the solution (blue line) 3 minutes. Photoexcitation was placed at 355 nm in both cases.

## X-ray photoelectron spectroscopy (XPS)

The valence state of the protein-stabilized AuNCs synthesized by biomineralization was investigated by XPS. Figure S10 shows that the Au core was mainly composed of Au (0). The XPS spectrum of C8-24Cys-AuNCs synthesized through the biomineralization-inspired procedure showed a peak at the binding energy of 83.7 eV (Au $4f_{7/2}$) (Figure S11).

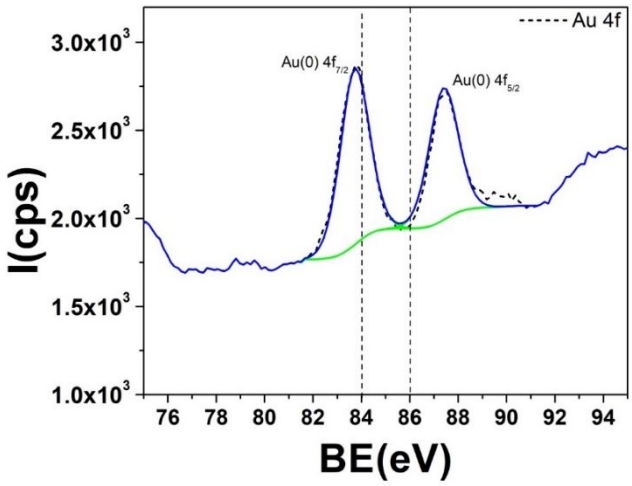


**Figure S11.** XPS spectrum of C8-24Cys-AuNCs synthesized by biomineralization.

**Characterization of the Prot-AuNCs synthesized with tryptophan containing proteins (2nd stage of protein engineering)**

**MALDI-TOF MS**

**Table S6.** Determination of the number of Au atoms in the Prot-AuNCs synthesized with the Trp containing proteins by MALDI-TOF.

| Sample | MALDI-TOF | | |
|---|---|---|---|
| | MSC[a] | FWHM[b] | NMA[c] |
| Reduction agent-assisted procedure | | | |
| C8-24Cys | 33459.51 | 156 | -- |
| C8-24Cys-AuNCs | 37565.89 | 1361 | 21±7 |
| C8-24Cys-16Trp | 34264.98 | 531 | -- |
| C8-24Cys-16Trp-AuNCs | 38375.86 | 1399 | 21±7 |
| Biomineralization-inspired procedure | | | |
| C8-24Cys | 33459.51 | 156 | -- |
| C8-24Cys-AuNCs | 38271.98 | 1398 | 24±7 |
| C8-24Cys-16Trp | 34264.98 | 531 | -- |
| C8-24Cys-16Trp-AuNCs | 39063.16 | 1417 | 24±7 |

*[a]Center of mass peak in Daltons (MSC). [b]Full width at half maximum in Daltons (FWHM). [c] Number of metal atoms per cluster (NMA).*

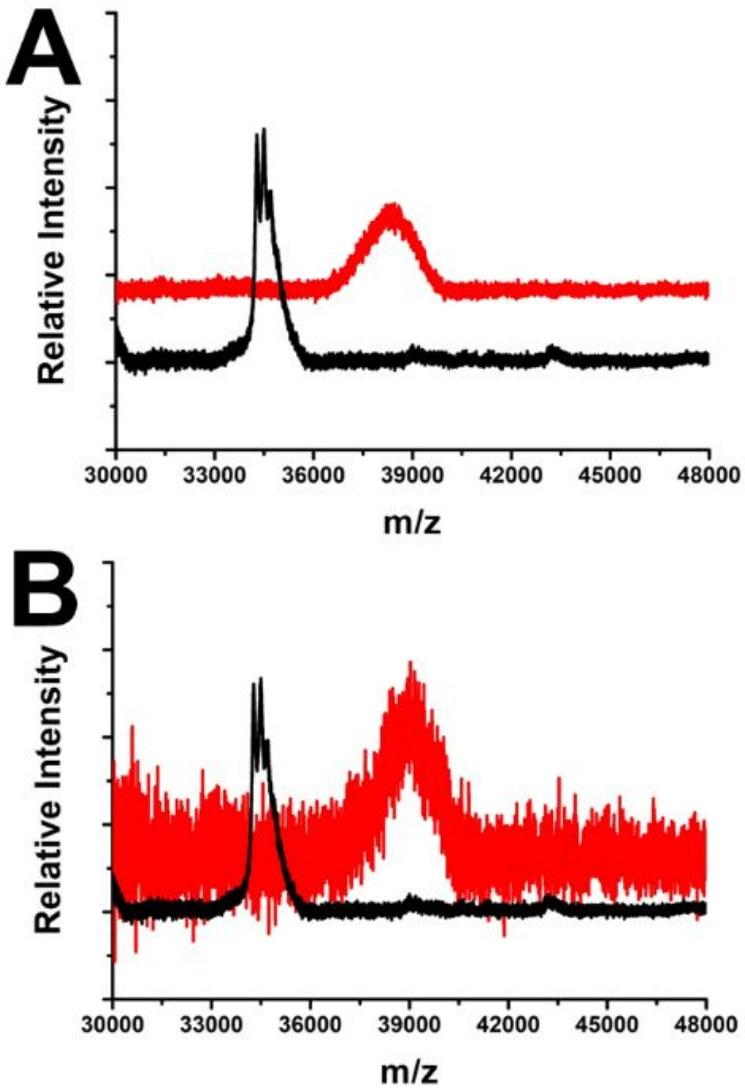


**Figure S12.** MALDI-TOF mass spectra of C8-24Cys-16Trp protein (black lines) and C8-24Cys-16Trp-AuNCs (red lines) synthesized through reduction (**A**) and biomineralization (**B**).

**Scanning Transmission Electron Microscopy (HAADF-STEM)**

The size and morphology of C8-24Cys-16W-AuNCs synthesized through reduction and biomineralization were evaluated by scanning transmission electron microscopy (STEM), taking advantage of the chemical contrast of Au obtained in high-angle annular dark field (HAADF) (Figure S13A). Indeed, C4-8Cys-16W-AuNCs synthesized through reduction and biomineralization showed NCs with an average diameter of 1.2 ± 0.3 nm and 1.5 ± 0.3 nm, respectively (Figure 13B). This size regime is accordant with the size range of previously reported fluorescent AuNCs.[9, 10]

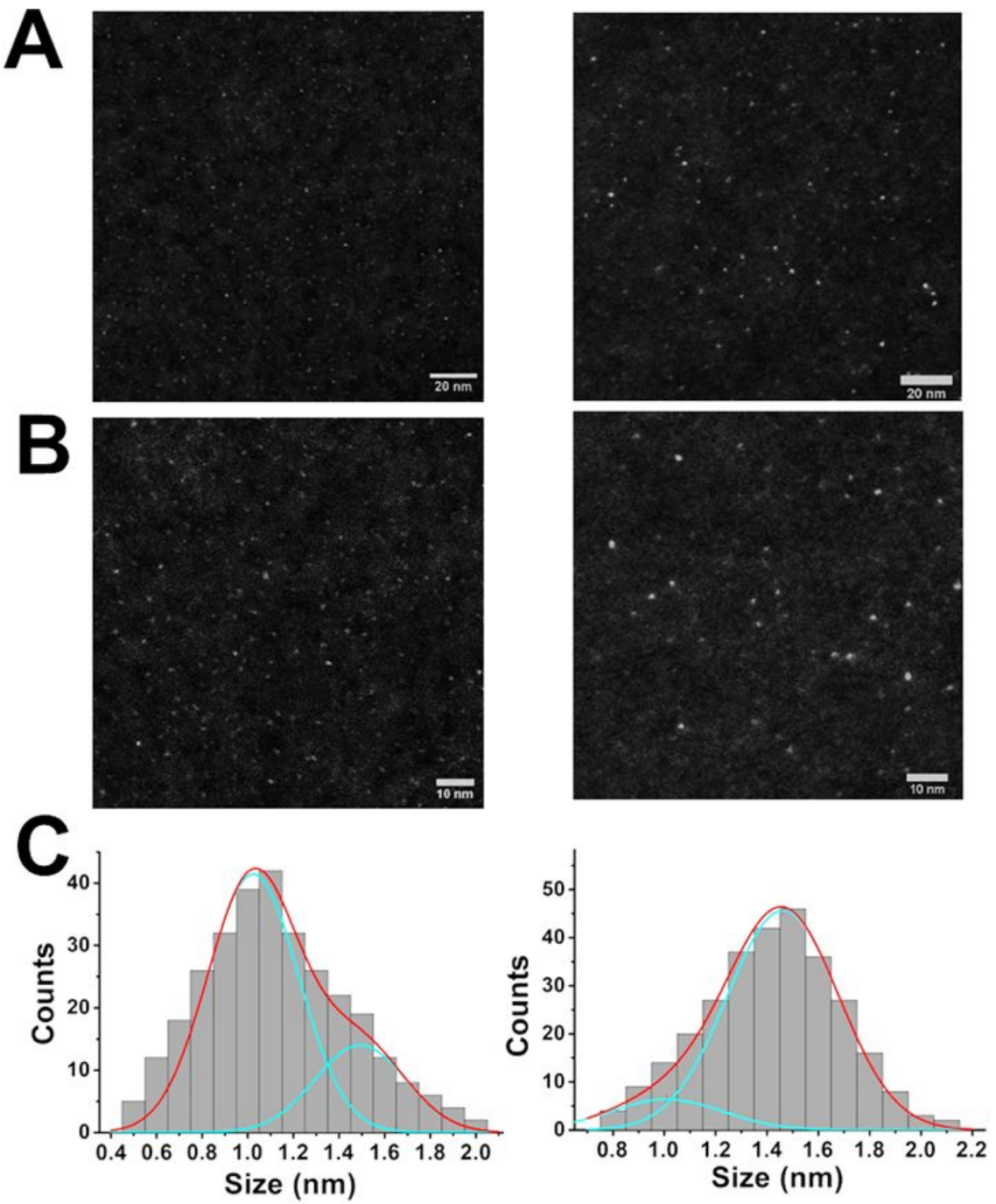


**Figure S13**. (A-B) HAADF STEM images of C8-24Cys-16W-AuNCs synthesized through reduction (left) and the biomineralization (right). Scale bar: 10nm. (C) Size distribution histogram C8-24Cys-16W-AuNCs synthesized through reduction (left) and biomineralization (right) measured from STEM micrographs. The histogram was fitted to a two-component Gaussian distribution (R-squared = 0.99).

**Circular Dichroism (CD)**

The structural integrity of the C8-24Cys-16W protein upon AuNCs synthesis through reduction and biomineralization, critical for future applications, was monitored by circular dichroism (CD). CD spectra of the C8-24Cys-16W-AuNCs synthesized through reduction (Figure S14**A**) and C8-24Cys-16W-AuNCs synthesized through biomineralization (Figure S14**B**) showed that the C8-24Cys-16W protein retained α-helical structure, indicating that the synthesis of AuNCs through both procedures did not affect the structure of the scaffolds (Figure S14).

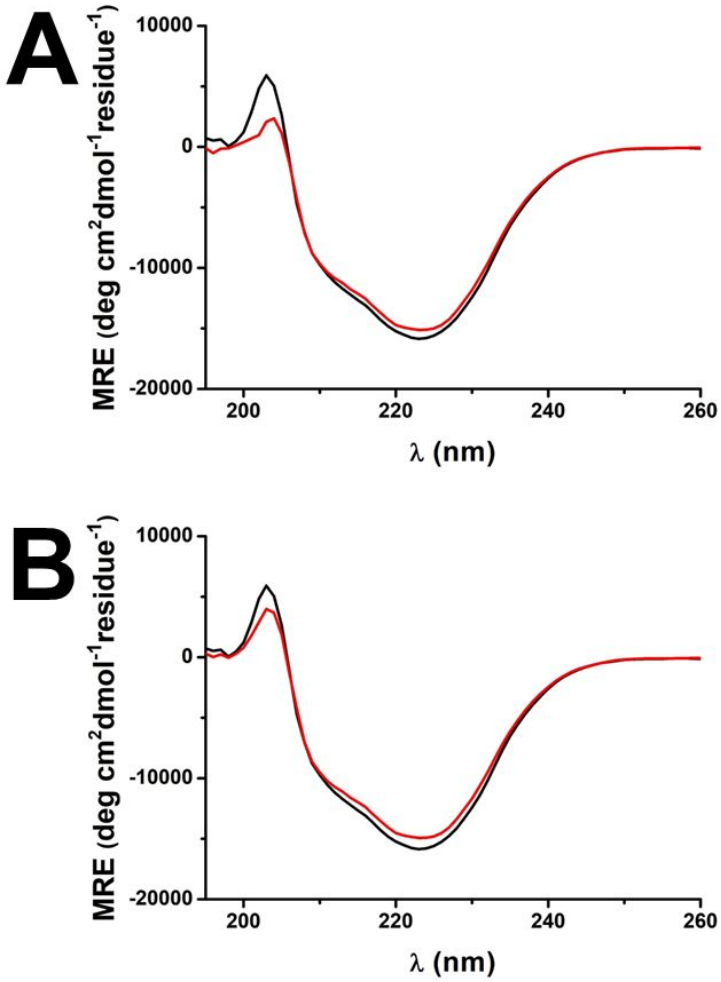


**Figure S14.** CD spectra of C8-24Cys-16W protein (black line) and, C8-24Cys-16W-AuNCs synthesized through reduction (**A**) and C8-24Cys-16W-AuNCs synthesized through biomineralization (**B**) (red line).

## Time-resolved Photoluminescence Measurements

**Table S7**. PL decay parameters for the different Prot-AuNCs.

| AuNCs | A1 | τ1 | A2 | τ2 | A3 | τ3 | < τ > |
|---|---|---|---|---|---|---|---|
| C8-24Cys-16W (reduction) $\lambda_{em}$ 463 nm | 91% | 0.16 ns | 8% | 1.49 ns | 1% | 5.65 ns | 0.33 ns |
| C8-24Cys-16W (reduction) $\lambda_{em}$ 670 nm | 54% | 0.17 μs | 33% | 1.20 μs | 13% | 5.21 μs | 1.15 μs |
| C8-24Cys-16W (biomineralization) $\lambda_{em}$ 460 nm | 74% | 0.23 ns | 21% | 2.16 ns | 4% | 13.64 ns | 1.22 ns |
| C8-24Cys-16W (biomineralization) $\lambda_{em}$ 670 nm | 22% | 0.43 μs | 62% | 1.93 μs | 16% | 3.91 μs | 1.93 μs |

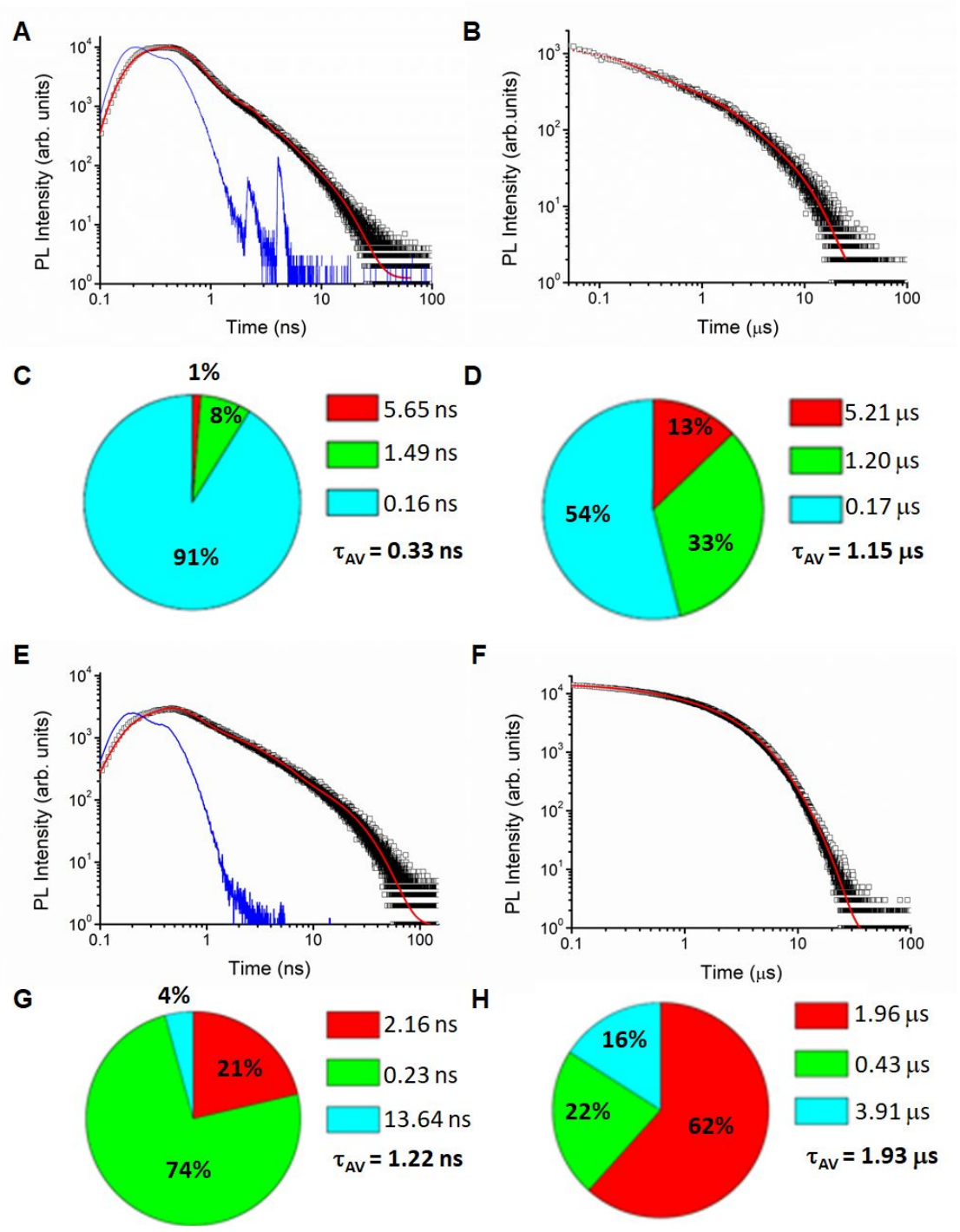


**Figure S15.** The photoluminescence lifetime analysis of C8-24Cys-16W-AuNCs. PL decay curves with corresponding three-exponential fits depicted by a red solid line of samples synthesized by reduction photoexcited at 405 nm and detected at 463 nm (A) and photoexcited at 355 nm and detected at 670 nm (B). Corresponding statistical distributions of the decay components are depicted in C and D respectively. PL decay curves with corresponding three-exponential fits depicted by a red solid line of samples synthesized by biomineralization detected photoexcited at 405 nm and detected at 460 nm (C) and photoexcited at 355 nm and detected at 670 nm (D) with statistical distributions of the decay components in G and H. Nanosecond PL decay fits were deconvoluted by the instrumental response function (blue decay curve in A and E).

**X-ray photoelectron spectroscopy (XPS)**

The valence state of the Prot-AuNCs was investigated by XPS. Figure S15 shows that the Au core in C8-24Cys-16W-AuNCs synthesized by reduction was mainly composed of Au(I) and Au(0) (59:41), while in C8-24Cys-AuNCs synthesized through biomineralization was mainly composed of Au (0). The XPS spectra of C8-24Cys-16W-AuNCs synthesized by reduction and biomineralization showed peaks at the binding energy of 84.5 and 83.8 eV (Au $4f_{7/2}$), respectively (Figure S16).

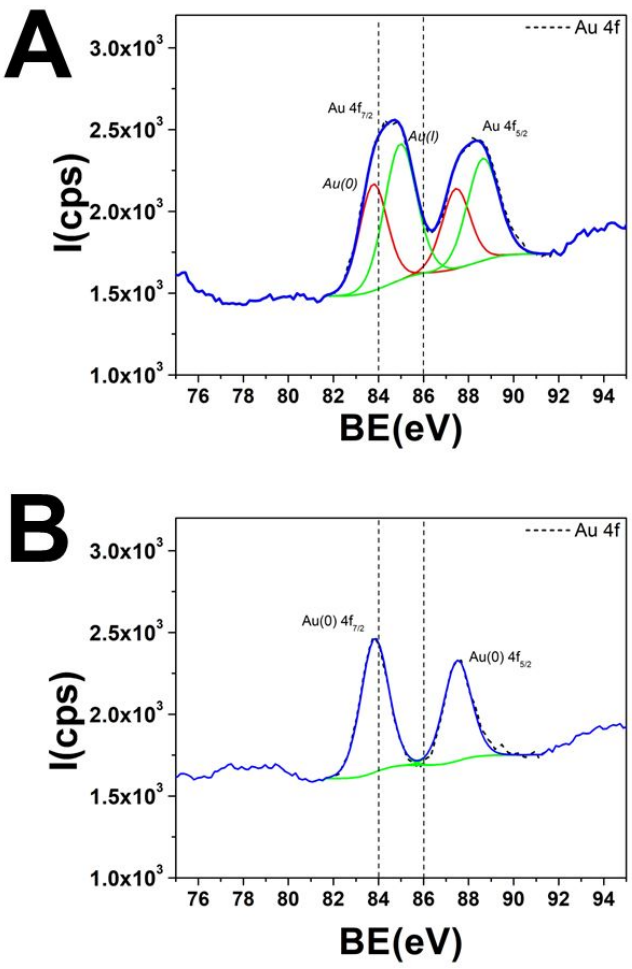


**Figure S16.** XPS spectrum of C8-24Cys-16W-AuNCs synthesized by reduction (**A**) and biomineralization (**B**).

**Study of energy transfer phenomenon from Trp residues to AuNCs**

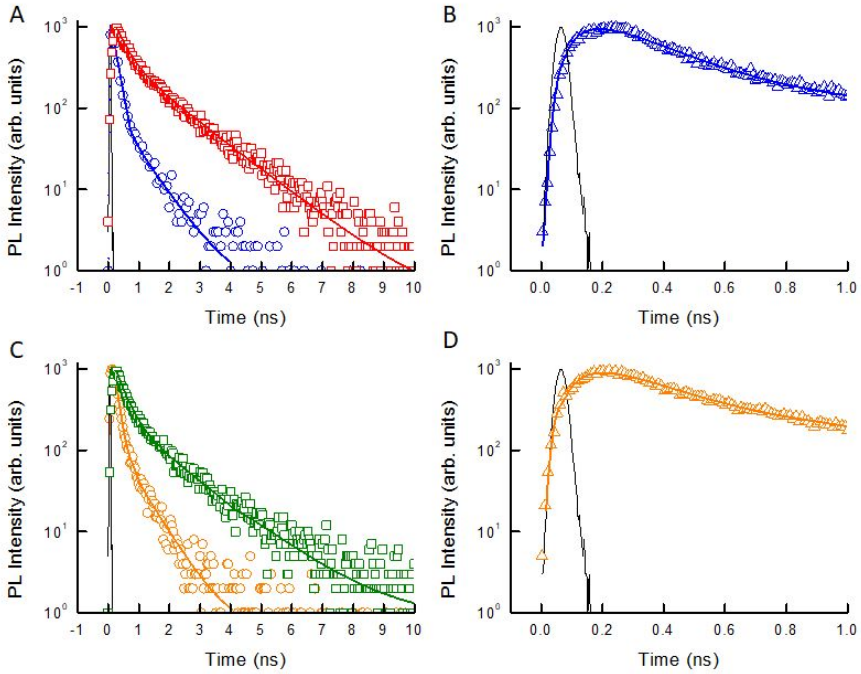


**Figure S17.** Characterization of energy transfer between Trps and AuNCs. (A) PL decay of Trp emission in C8-24Cys (red squares) and in C8-24Cys-AuNCs (blue circles) with corresponding fits ($\lambda_{em}$ 380 nm). (B) PL build-up of C8-24Cys-AuNC emission ($\lambda_{em}$ 444 nm, blue triangles) upon predominant Trp photoexcitation with fit (blue line). (C) PL decay of Trp emission in C8-24Cys-16W (green squares) and in C8-24Cys-16W-AuNCs (orange circles) with corresponding fits ($\lambda_{em}$ 380 nm). (D) PL build-up of C8-24Cys-16W-AuNC ($\lambda_{em}$ 444 nm, orange triangles) upon Trp photoexcitation with fit (orange line). Picosecond PL decay times were obtained from fits upon deconvolution of the instrumental response function (black decay curves in A-D). Photoexcitation was carried out with 120 fs pulses at 258 nm in all cases.

**Table S8.** PL decay parameters of C8-24cys, C8-24cys-16W proteins and the different protein-stabilized AuNCs upon photoexcitation at 258 nm. E stands for the energy transfer efficiency.

| **Sample** | **$A_1$(%)** | **$t_1$(ns)** | **$A_2$(%)** | **$t_2$(ns)** | **$A_3$ (%)** | **$t_3$ (ns)** | **$t_{av}$(ns)** | **E** |
|---|---|---|---|---|---|---|---|---|
| **C8-24Cys-protein λem 380 nm** | 39 | 1.51 | 61 | 0.36 | - | - | 0.81 | -- |
| **C8-24Cys-AuNCs (reduction) λem 380 nm** | 16 | 0.66 | 84 | 0.14 | - | - | 0.23 | 0.72 |
| **C8-24Cys-AuNCs (reduction)** | 4 | 1.40 | 46 | 0.18 | 50 | 0.09 | 0.28 | 0.086 |

| | | | | | | | | |
|---|---|---|---|---|---|---|---|---|
| **λem 444 nm** | | | | | | | | |
| **C8-24Cys-AuNCs (Biomineralization)** **λem 380 nm** | 35 | 1.16 | 65 | 0.28 | - | - | 0.59 | 0.27 |
| **C8-24cys-16W-protein** **λem 380 nm** | 28 | 1.47 | 72 | 0.30 | - | - | 0.63 | -- |
| **C8-24cys-16W-AuNCs (reduction)** **λem 380 nm** | 13 | 0.72 | 87 | 0.17 | - | - | 0.24 | 0.61 |
| **C8-24cys-16W-AuNCs (reduction)** **λem 444 nm** | 4 | 1.84 | 46 | 0.21 | 50 | 0.09 | 0.34 | |
| **C8-24cys-16W-AuNCs (Biomineralization)** **λem 380 nm** | 29 | 1.21 | 71 | 0.30 | - | - | 0.56 | 0.11 |

### 3.3.7. Tryptophan fluorescence quenching studies

The Tryptophan fluorescence quenching of C8-24cys and C8-24cys-16W protein scaffolds and, C8-24cys-AuNCs and C8-24cys-16W-AuNCs by acrylamide at different concentrations (0-0.2 M) were evaluated in 50 mM phosphate 150 mM NaCl pH 7.4 at 20 °C (Figure S18, Table S9).

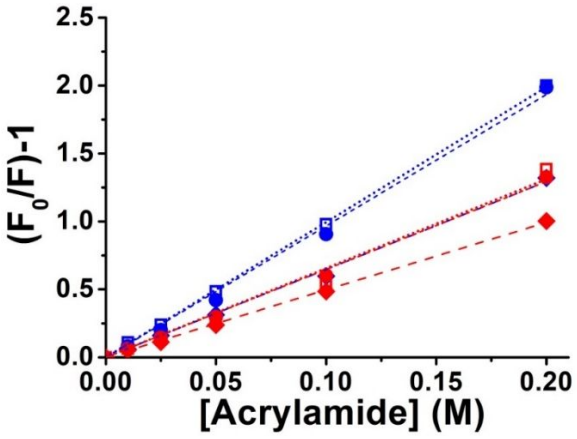


**Figure S18.** Stern-Volmer plot showing tryptophan fluorescence quenching in CTPR proteins and Prot-AuNCs. Tryptophan fluorescence quenching of C8-24cys (empty blue squares), C8-24cys-16W (empty red squares), C8-24cys-AuNCs synthesized by reduction and biomineralization, (filled blue rhombus and filled blue circles, respectively), and C8-24cys-16W-AuNCs synthesized by reduction and

biomineralization (filled red rhombus filled red circles, respectively), by acrylamide in 50 mM phosphate 150 mM NaCl pH 7.4 at 20 °C. Photoexcitation was placed at 280 nm.

**Table S9.** Comparison of Ksv values for the quenching of PL intensity of Trp, in the protein scaffolds and Prot-AuNCs, by acrylamide.

| Sample | Ksv ($M^{-1}$) | r | S.D. |
|---|---|---|---|
| C8-24cys protein | 9.95 | 0.999 | 0.05 |
| C8-24cys-16W protein | 6.55 | 0.998 | 0.18 |
| C8-24cys-AuNCs (RAAP) | 6.46 | 0.998 | 0.11 |
| C8-24cys-16W-AuNCs (RAAP) | 4.96 | 0.999 | 0.04 |
| C8-24cys-AuNCs (BIP) | 9.67 | 0.997 | 0.21 |
| C8-24cys-16W-AuNCs (BIP) | 6.47 | 0.997 | 0.12 |

r is the correlation coefficient and S.D. is the standard deviation.

**Effect of the Trp fluorescence quenching on the PL of the Prot-AuNCs**

The effect of the Trp fluorescence quenching on the photoluminescence emission of the Prot-AuNCs was investigated at increasing acrylamide concentrations (0-0.2 M). For this purpose, the photoluminescence intensity of the high energy band of the Prot-AuNCs synthesized by reduction (450 nm, Figure S19A-B) and low energy band of Prot-AuNCs synthesized by biomineralization (680 nm, Figure S19C-D) were monitored using an excitation wavelength of 280 nm, and at other two excitation wavelengths farther away from the direct excitation of the Trp (Table S10).

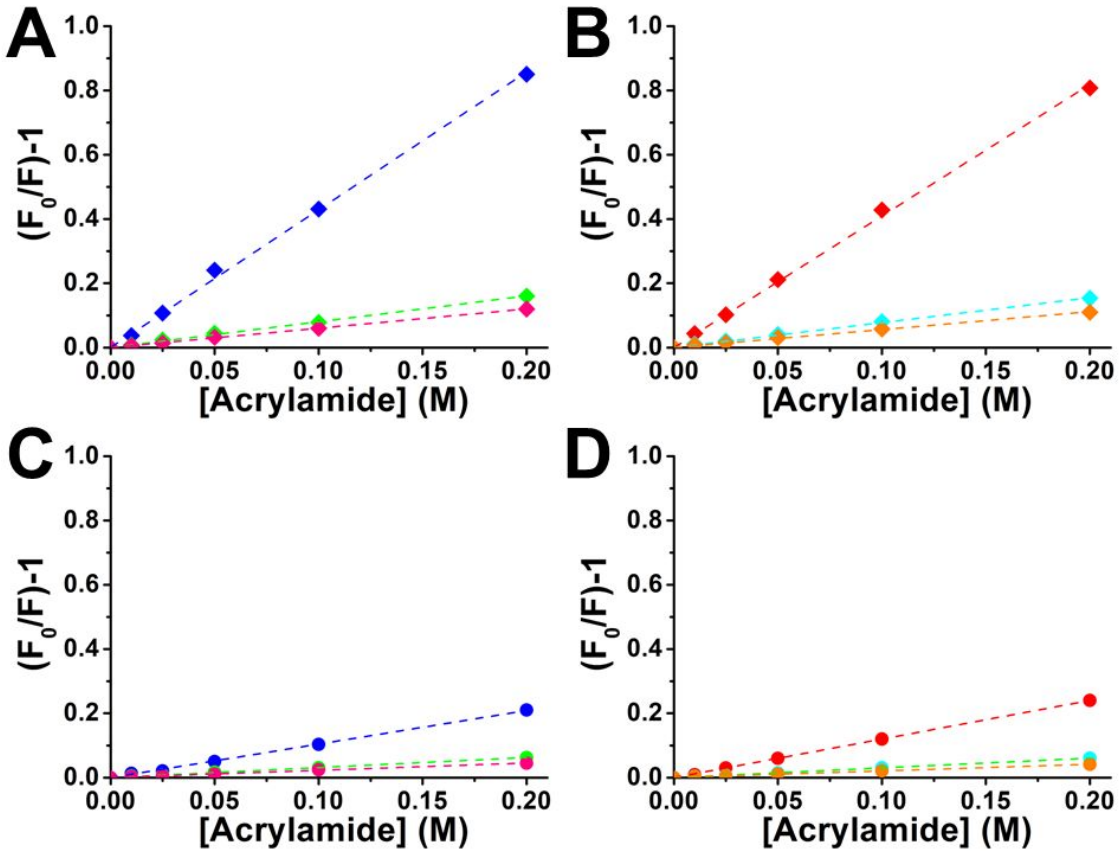


**Figure S19.** Stern-Volmer plot showing the effect of the tryptophan quenching on the PL properties of the Prot-AuNCs by acrylamide in 50 mM phosphate 150 mM NaCl pH 7.4 at 20 °C. **A.** PL intensities monitored at 450 nm of C8-24cys-AuNCs synthesized by reduction under photoexcitation at 280 nm (blue rhombus), 360 nm (green rhombus) and 400 nm (pink rhombus). **B.** PL intensities monitored at 450 nm of C8-24cys-16W-AuNCs synthesized by reduction under photoexcitation at 280 nm (red rhombus), 360 nm (cyan rhombus) and 400 nm (orange rhombus). **C**. PL intensities monitored at 680 nm of C8-24cys-AuNCs synthesized by biomineralization under photoexcitation at 280 nm (blue circles), 360 nm (green circles) and 400 nm (pink circles). **D.** PL intensities monitored at 680 nm of C8-24cys-16W-AuNCs synthesized by biomineralization under photoexcitation at 280 nm (red circles), 360 nm (cyan circles) and 400 nm (orange circles).

**Table S10.** Effect of the Trp fluorescence quenching on the fluorescent emission of the Prot-AuNCs, investigated at increasing acrylamide concentrations (0-0.2M).

| **Sample** | **$\lambda_{excitation}$ (nm)** | **Ksv ($M^{-1}$)** | ***r*** | **S.D.** |
|---|---|---|---|---|
| C8-24cys-AuNCs (Reduction) | 280 | 4.29 | 0.99906 | 0.054 |
| | 360 | 0.80 | 0.99849 | 0.013 |
| | 400 | 0.60 | 0.99969 | 0.005 |

| | | | | |
|---|---|---|---|---|
| C8-24cys-16W-AuNCs (Reduction) | 280 | 4.09 | 0.99929 | 0.045 |
| | 360 | 0.78 | 0.99910 | 0.010 |
| | 400 | 0.56 | 0.99853 | 0.009 |
| C8-24cys-AuNCs (Biomineralization) | 280 | 1.04 | 0.99917 | 0.012 |
| | 360 | 0.31 | 0.99834 | 0.006 |
| | 400 | 0.23 | 0.99814 | 0.005 |
| C8-24cys-16W-AuNCs (Biomineralization) | 280 | 1.20 | 0.99986 | 0.006 |
| | 360 | 0.30 | 0.99954 | 0.004 |
| | 400 | 0.21 | 0.99924 | 0.005 |

*r* is the correlation coefficient and S.D. is the standard deviation.

## References


1. Main, E. R.; Xiong, Y.; Cocco, M. J.; D'Andrea, L.; Regan, L. *Structure* **2003,** 11, (5), 497-508.
2. Kajander, T.; Cortajarena, A. L.; Main, E. R.; Mochrie, S. G.; Regan, L. *Journal of the American Chemical Society* **2005,** 127, (29), 10188-90.
3. Cortajarena, A. L.; Mochrie, S. G.; Regan, L. *Protein Science* **2011,** 20, (6), 1042-1047.
4. Couleaud, P.; Adan-Bermudez, S.; Aires, A.; Mejías, S. H.; Sot, B.; Somoza, A.; Cortajarena, A. L. *Biomacromolecules* **2015,** 16, (12), 3836-3844.
5. Aires, A.; Lopez-Martinez, E.; Cortajarena, A. L. *Biosensors* **2018,** 8, (4), 110.
6. Aires, A.; Llarena, I.; Moller, M.; Castro-Smirnov, J.; Cabanillas-Gonzalez, J.; Cortajarena, A. L. *Angewandte Chemie International Edition* **2019,** 58, (19), 6214-6219.
7. Aires, A.; Fernández-Luna, V.; Fernández-Cestau, J.; Costa, R. D.; Cortajarena, A. L. *Nano Letters* **2020**, *20*, 2710-2719.
8. Xie, J.; Zheng, Y.; Ying, J. Y. *Journal of the American Chemical Society* **2009,** 131, (3), 888-889.
9. Kawasaki, H.; Hamaguchi, K.; Osaka, I.; Arakawa, R. *Advanced Functional Materials* **2011,** 21, (18), 3508-3515.
10. Ding, H.; Li, H.; Wang, X.; Zhou, Y.; Li, Z.; Hiltunen, J. K.; Shen, J.; Chen, Z. *Chemistry of Materials* **2017,** 29, (19), 8440-8448.